IOPscience iopscience.iop.org

Home Search Collections Journals About Contact us My IOPscience

Estimating the fracture density of small-scale vertical fractures when large-scale vertical fractures are present

This content has been downloaded from IOPscience. Please scroll down to see the full text.

2015 J. Geophys. Eng. 12 311

(http://iopscience.iop.org/1742-2140/12/3/311)

View the table of contents for this issue, or go to the journal homepage for more

Download details:

IP Address: 18.83.2.4
This content was downloaded on 15/04/2015 at 16:53

Please note that terms and conditions apply.

IOP Publishing Journal of Geophysics and Engineering
J. Geophys. Eng. **12** (2015) 311–320 doi:10.1088/1742-2132/12/3/311

Estimating the fracture density of small-scale vertical fractures when large-scale vertical fractures are present

Yuwei Liu[1], Ning Dong[1], Mike Fehler[2], Xinding Fang[2] and Xiwu Liu[1]

[1] Petroleum Exploration and Production Research Institute, Sinopec, Beijing 100083, People's Republic of China
[2] MIT, Boston, MA 02139, USA

E-mail: liuyw.syky@sinopec.com

Received 7 August 2014, revised 29 December 2014
Accepted for publication 19 January 2015
Published 14 April 2015

Abstract

Fractures in reservoirs significantly affect reservoir flow properties in subsequent years, which means that fracture characteristics such as preferred orientation, crack density or fracture compliance, what filling is in the fractures and so on are of great importance for reservoir development. When fractures are vertical, aligned and their dimensions are small relative to the seismic wavelength, the medium can be considered to be an equivalent horizontal transverse isotropic (HTI) medium. However, geophysical data acquired over naturally fractured reservoirs often reveal the presence of multiple fracture sets. We investigate a case where there are two vertical sets of fractures having differing length scales. One fracture set has length scale that is much smaller than the seismic wavelength but the other has length scale that is similar to the seismic wavelength. We use synthetic data to investigate the ability to infer the properties of the small-scale fractures in the presence of the large-scale fracture set. We invert for the Thomsen-type anisotropic coefficients of the small-scale fracture set by using the difference of the P wave amplitudes at two azimuths, which makes the inversion convex. Then we investigate the influence of the presence of the large-scale fractures on our ability to infer the properties of the small-scale fracture set. Surprisingly, we find that we can reliably infer the fracture density of the small-scale fractures even in the presence of large-scale fractures having significant compliance values. Although the inversion results for Thomsen-type anisotropic coefficients of small-scale fractures for one model are not good enough to figure out whether it is gas-filled or fluid-filled, we can find a big change of Thomsen-type anisotropic coefficient $\varepsilon^{(V)}$ between the models in which small-scale fractures are filled with gas and fluid.

Keywords: AVAZ, small-scale vertical fracture, large-scale vertical fracture, crack density, fracture compliance

(Some figures may appear in colour only in the online journal)

1. Introduction

Natural or man-made fractures often present in petroleum reservoirs and play a significant role in oil-bearing and migration pathways. The good understanding of fracture characteristics is of great practical importance for activities like forecasting reservoir performance, mine and well stability, and carbon dioxide sequestration.

There are several approaches for modeling the seismic response of fractured media (Liu *et al* 2000). The effective medium approach is most commonly used when fracture dimensions and spacings are small relative to the seismic wavelength. The Hudson theory (Hudson 1980, 1981, 1996) is a model for isolated oblate spheroidal penny-shaped cracks embedded in an isotropic solid where the short axis of ellipsoids is equal to the fracture aperture and the long axis is equal to

 © 2015 Sinopec Geophysical Research Institute Printed in the UK

the fracture length. The linear-slip theory (Schoenberg 1980, 1983) considers fractures as planes of weakness with non-welded boundary conditions and has an excess compliance that leads to an effective compliance tensor of the medium. Then the background and fracture parameters can be related to the Thomsen-type anisotropic coefficients (Rüger 1997, Thomsen 1986, 1988, 1995), which describe the influence of anisotropy on various seismic signatures. When fractures are much larger than the seismic wavelength, the fractures will scatter the incident seismic waves and generate complex waveform codas.

We cannot directly image the fractures from seismic measurements, but various seismic attributes can give us information about fracture orientation, intensity (fracture density or normal and tangential compliance) and sometimes what fluid is in the fractures and hence to characterize fractured reservoirs (Hall and Kendall 2003, Luo and Evans 2004, Jakobsen *et al* 2007). Rocks with vertical cracks or fractures can be considered as equivalent HTI media. Well-developed methods for characterizing HTI media from seismic data are shear wave splitting and AVAZ (amplitude variation with offset and azimuth) when wavelength is much larger than fracture dimension (Gutierrez 2009). Scattered waves can provide information to extract fracture properties when the wavelength is approximately the fracture dimension (Fang *et al* 2013b). However, when fracture sets having differing orientations exist, the seismic amplitude response will be more complicated. In this paper, we assume that the isotropic host rock has two vertical sets of fracture with differing length scales. Analysis of the variation of reflectivity as a function of both azimuth and incident angle can provide information about the subsurface small-scale fracture anisotropy when wavelength is much larger than the small-scale fracture dimension but approximate to large-scale fracture dimension. Once Thomsen-type anisotropic parameters are extracted, the fracture density can be determined (Liu *et al* 2012). To identify the small-scale fracture density by seismic reflection data, it is useful to compare the inversion results for models with different large-scale fracture compliance.

2. Theory and methods

The compressional plane wave reflection coefficient for an HTI medium can be described as a function of the polar incident angle θ and azimuthal phase angle φ relative to the symmetry axis in the approximate form as (Rüger and Tsvankin 1995, Rüger 1996, 1997)

$$\begin{aligned} R \approx \frac{1}{2}\frac{\Delta Z}{\overline{Z}} + \frac{1}{2}\Bigg\{ & \frac{\Delta\alpha}{\overline{\alpha}} - \left(\frac{2\overline{\beta}}{\overline{\alpha}}\right)^2 \frac{\Delta G}{\overline{G}} \\ & + \left[\Delta\delta^{(V)} + 2\left(\frac{2\overline{\beta}}{\overline{\alpha}}\right)^2 \Delta\gamma\right]\cos^2\varphi\Bigg\}\sin^2\theta \\ & + \frac{1}{2}\left\{\frac{\Delta\alpha}{\overline{\alpha}} + \Delta\varepsilon^{(V)}\cos^4\varphi + \Delta\delta^{(V)}\sin^2\varphi\cos^2\varphi\right\} \\ & \sin^2\theta\tan^2\theta \end{aligned} \tag{1}$$

where α and β are the isotropy-plane velocities of P- and S-wave, respectively. G is the vertical shear modulus and $G = \rho\beta^2$ corresponds to the vertically propagating S-wave. $Z = \rho\alpha$ is the vertical P-wave impedance. The '—' means average quantities e.g. $\overline{Z} = Z_2 + Z_1/2$ and 'Δ' is the differences between lower and upper medium parameters e.g. $\Delta Z = Z_2 - Z_1$. The index 1 corresponds to the upper medium and the index 2 to the lower medium.

$$\gamma^{(V)} = -\frac{\gamma}{1+2\gamma} \tag{2}$$

where γ is the generic Thomsen parameter. $\gamma^{(V)}$, $\delta^{(V)}$, $\varepsilon^{(V)}$ are the Thomsen-type anisotropic coefficients for the HTI medium.

Choosing two azimuths φ and $\varphi+\eta$, the difference of their reflection coefficients ΔR for the same incident angle can be expressed as

$$\begin{aligned} \Delta R &= R(\varphi) - R(\varphi+\eta) \\ &= \Delta\gamma\left(\frac{2\overline{\beta}}{\overline{\alpha}}\right)^2 [\cos^2\varphi - \cos^2(\varphi+\eta)]\sin^2\theta \\ &+ \frac{1}{2}\delta^{(V)}\sin^2\theta\{[\cos^2\varphi - \cos^2(\varphi+\eta)] \\ &+ [\sin^2\varphi\cos^2\varphi - \sin^2(\varphi+\eta)\cos^2(\varphi+\eta)]\tan^2\theta\} \\ &+ \frac{1}{2}\Delta\varepsilon^{(V)}[\cos^4\varphi - \cos^4(\varphi+\eta)]\sin^2\theta\tan^2\theta. \end{aligned} \tag{3}$$

It is more direct to determine the Thomsen-type anisotropy parameters using equation (3) than equation (1) since terms involving α and β have dropped out, so we invert for Thomsen-type anisotropy parameters using the difference of data at two azimuths.

The inversion for anisotropy parameters from measured AVAZ data is done using a genetic algorithm. The cost function for the inversion is given by

$$\begin{aligned} \text{fitness} = & \sum_{i=1}^{I}\sum_{j=1}^{J}\omega_{ij} \\ & \sum_{k=1}^{K}\left[\Delta A(\varphi_i,\eta_j,\theta_k) - \frac{\Delta A_{\max}\Delta R(\varphi_i,\eta_j,\theta_k,\Delta\gamma,\Delta\delta^{(V)},\Delta\varepsilon^{(V)})}{\Delta R_{\max}}\right]^2 \\ & (i = 1,2,\ldots,I; j = 1,2,\ldots,J; k = 1,2,\ldots,K) \end{aligned} \tag{4}$$

where

$$\left|\Delta A(\varphi_i,\eta_j,\theta_k)\right| = \max\left|\Delta A\left(\varphi_i,\eta_j,\theta_k\right)\right|, (k = 1,2,\ldots,K) \tag{5}$$

A means measured reflection amplitude and ΔA is amplitude difference between azimuths φ and $\varphi+\eta$. ω_{ij} is a weighting coefficient. Then shear-wave splitting parameter $\gamma^{(V)}$ provides a way to quantify crack density e using (Bakulin *et al* 2000).

$$e = \frac{3(3-2g)\gamma^{(V)}}{8} \tag{6}$$

where $g = \beta^2/\alpha^2$, α and β are the background P- and S-wave velocities.

Table 1. Model parameters.

Parameter	First layer	Second layer	Second layer	Second layer	Third layer
Small-scale fracture	None	Gas	Water	Carbon dioxide	None
Depth	400 m	800 m	800 m	800 m	1000 m
γ	0	0.0974	0.0989	0.0989	0
$\delta^{(V)}$	0	−0. 1705	−0.1004	−0.1007	0
$\varepsilon^{(V)}$	0	−0.1635	−0.0039	−0.0045	0
α	4700 m s^{-1}	5200 m s^{-1}	5200 m s^{-1}	5200 m s^{-1}	4500 m s^{-1}
β	2450 m s^{-1}	3000 m s^{-1}	3000 m s^{-1}	3000 m s^{-1}	2240 m s^{-1}
ρ	2.4 g cm^{-3}	2.59 g cm^{-3}	2.59 g cm^{-3}	2.59 g cm^{-3}	2.3 g cm^{-3}
e	0	0.08	0.08	0.08	0

Note: Three models were studied by changing the properties of the fluid filling the fractures.

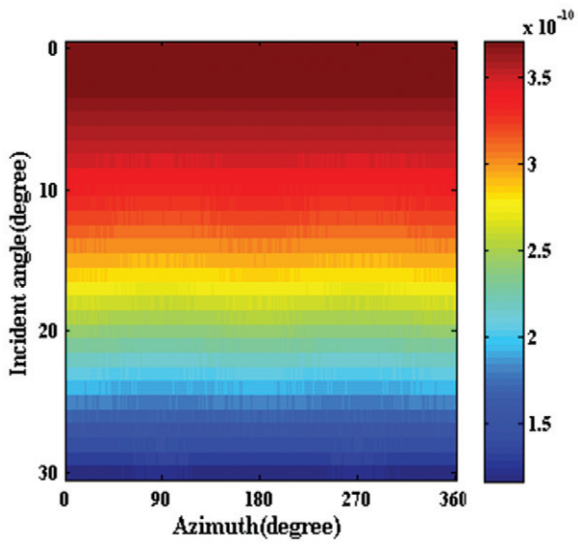

Figure 1. Reflection coefficient versus incident angle and azimuth for the HTI medium (small-scale fractures filled with gas) used for our study.

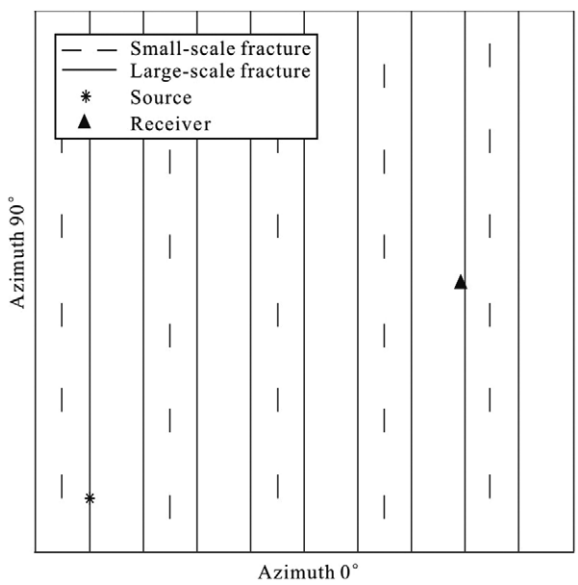

Figure 2. Sketch of the parallel fracture model. Offset and azimuth of receiver for traces shown in figure 9 are 400 m and 30 degrees, respectively.

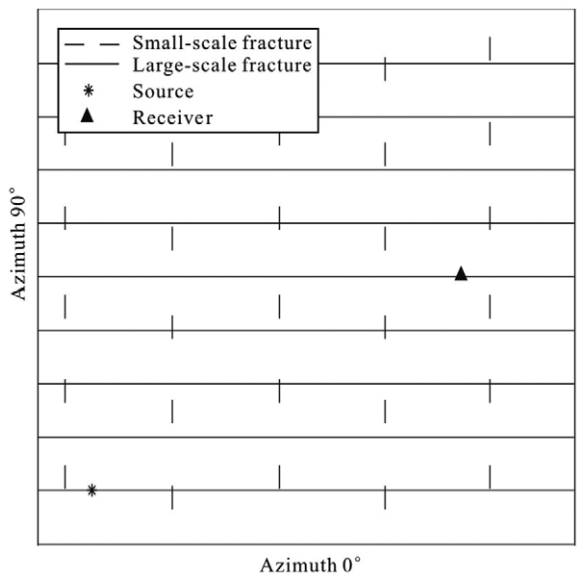

Figure 3. Sketch of the parallel fracture model. Offset and azimuth of receiver for traces shown in figure 10 are 400 m and 30°, respectively.

3. Model and synthetic data

Our model consists of three layers. The first and third layers are isotropic while the second one is an HTI medium equivalent to one containing vertical small-scale fractures whose properties are listed in table 1. The HTI medium properties are determined from the fracture properties using the Hudson theory and aspect ratio is 0.001. Figure 1 shows the variation of reflection response with incident angle and azimuth measured from synthetic data when there are just gas-filled small-scale fractures. The azimuthal variation in the reflection coefficients can be used to find the strike of the fractures. As azimuth increases from 0 degrees to 90 degrees, the reflection coefficient value decreases at the same incident angle in our example.

We add a set of vertical large-scale fractures to the second, HTI, medium and describe them by using the linear-slip theory. We assume the normal and tangential compliances of the large-scale fractures (Z_N and Z_T) are equal. What is more, the strike of the large-scale fractures is taken to be either parallel or perpendicular to that of the small-scale ones

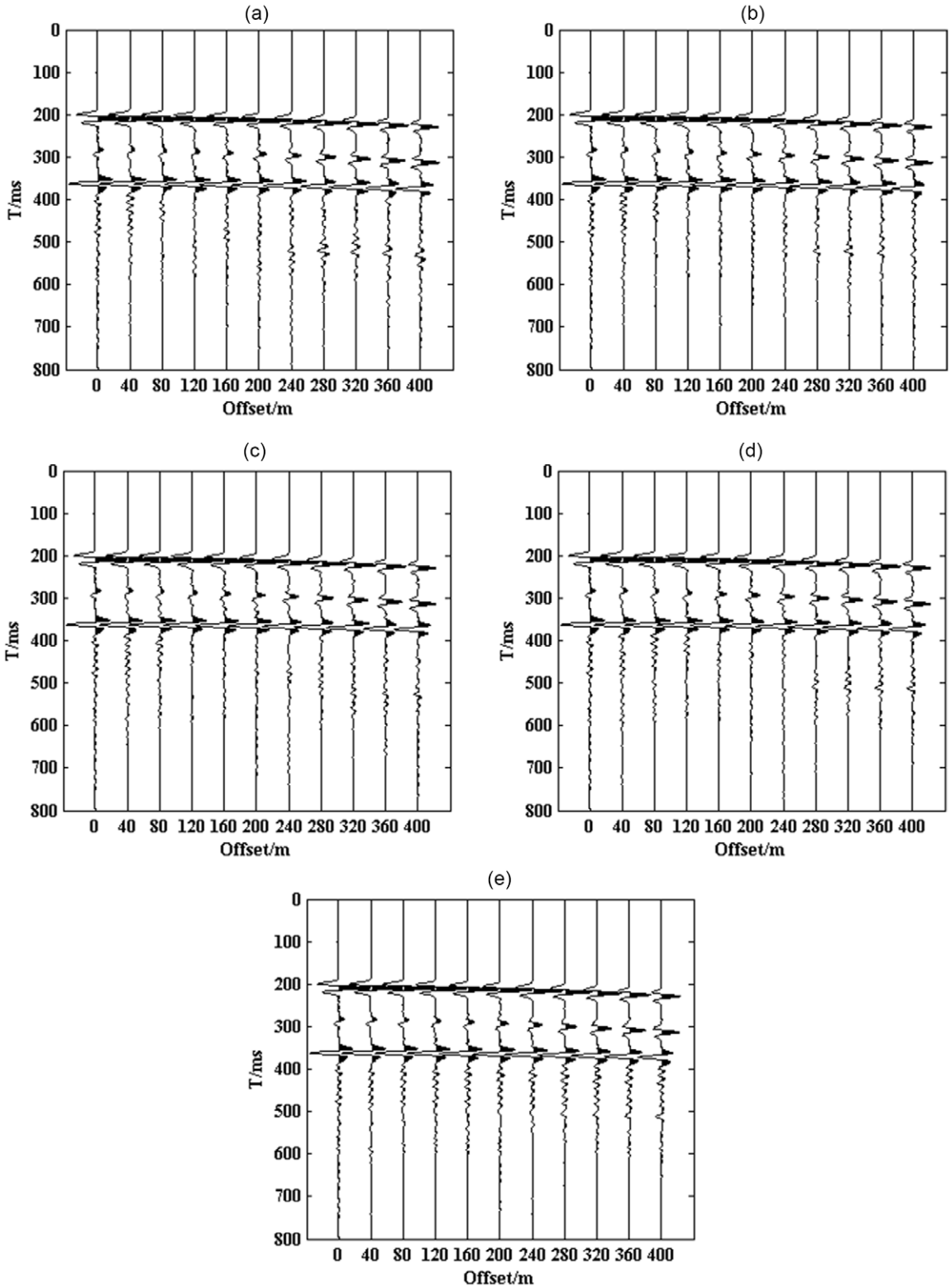

Figure 4. *Z*-component of motion for the P-wave reflected for the parallel fracture model. Large-scale fracture compliance is $0.1 \times 10^{-9}\,\mathrm{m\,Pa^{-1}}$ while small-scale fractures are gas-filled. Azimuth is defined in sketch of the parallel fracture model. (*a*) Azimuth 0°, (*b*) azimuth 30°, (*c*) azimuth 45°, (*d*) azimuth 60°, (*e*) azimuth 90°.

(figures 2 and 3). The large-scale fracture spacing is 50 m. We use a finite difference method (Coates and Schoenberg 1995, Fang *et al* 2013a) to generate synthetic data (figures 4 and 5). The scheme allows the simulation of the seismic response in a medium containing large-scale fractures embedded within a general HTI medium. We use a Ricker wavelet source with a center frequency of 40 Hz. Thickness of the upper layer is 400 m.

Figure 6 shows the reflection response measured from synthetic data when large-scale fracture normal and tangential compliance are $0.1 \times 10^{-9}\,\mathrm{m\,Pa^{-1}}$. Along the azimuth

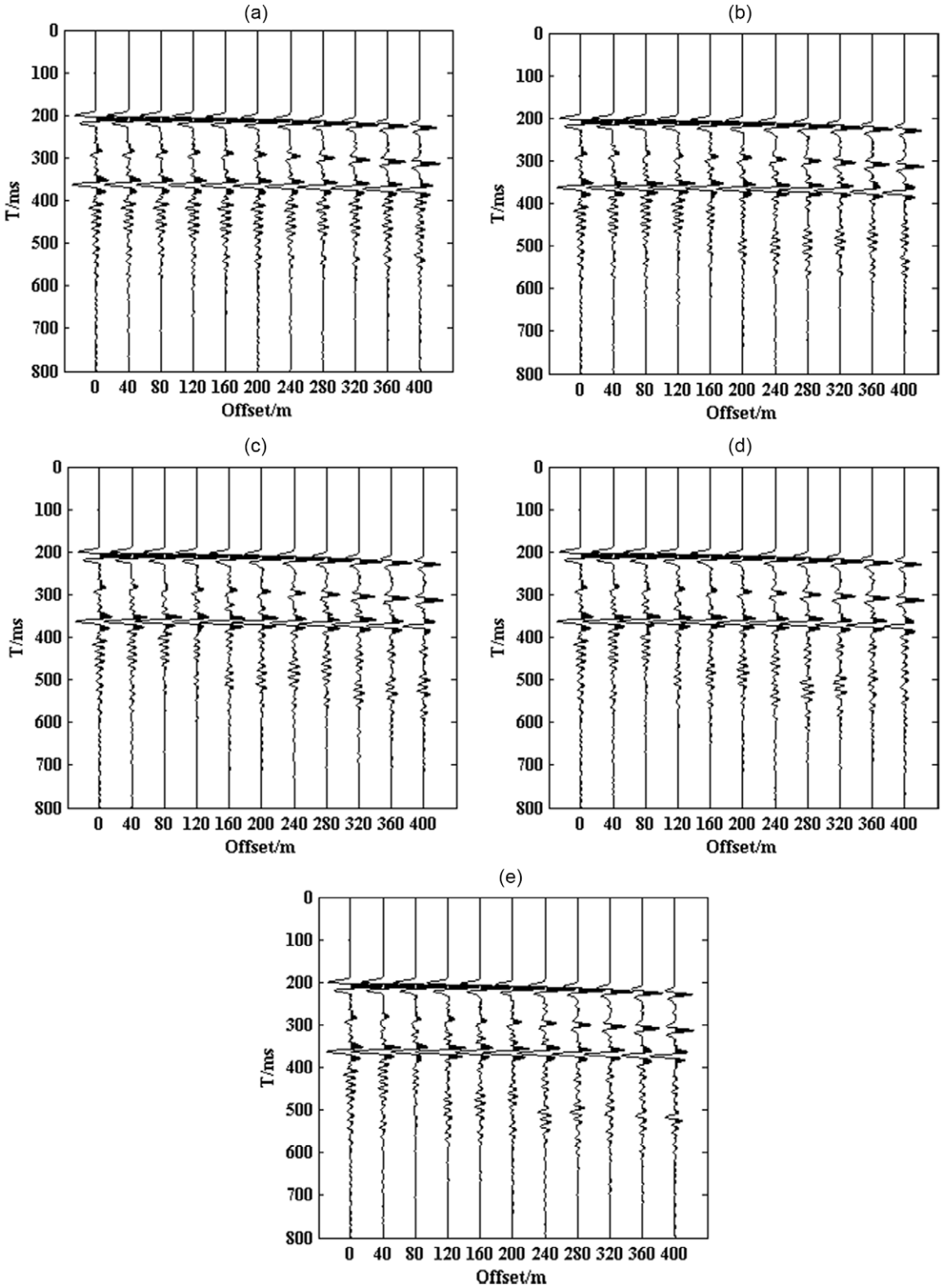

Figure 5. Same as figure 4 but for the perpendicular fracture model.

increases from 0 degrees to 90 degrees, the reflection amplitude measured from forward data decreases at the same incident angle for the parallel fracture model, so the variation of reflection response with azimuth still works well to estimate small-scale fracture strike.

When we compare the reflection amplitude for the model that has large-scale fractures with those for a model that does not include large-scale fractures, we find that they are different when large-scale fracture compliance is $0.1 \times 10^{-9}\,\mathrm{m\,Pa^{-1}}$. We assume that the differences are caused by large-scale

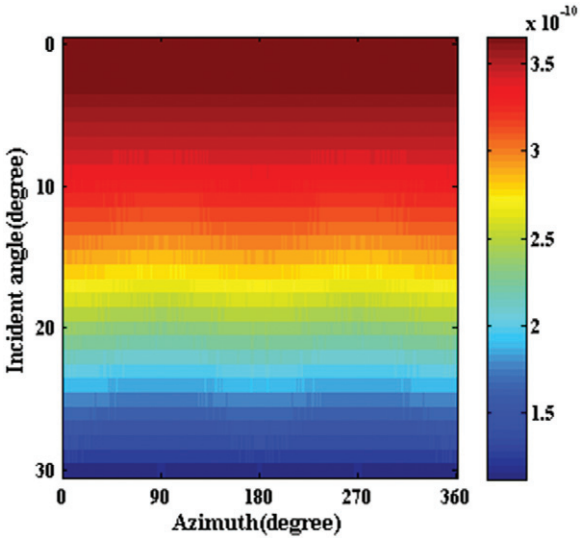

Figure 6. Reflection response versus incident angle and azimuth for the parallel model with large-scale compliance of $0.1 \times 10^{-9}\,\mathrm{m\,Pa^{-1}}$ (small-scale fractures are gas-filled). The response was derived from the *Z*-component of the data.

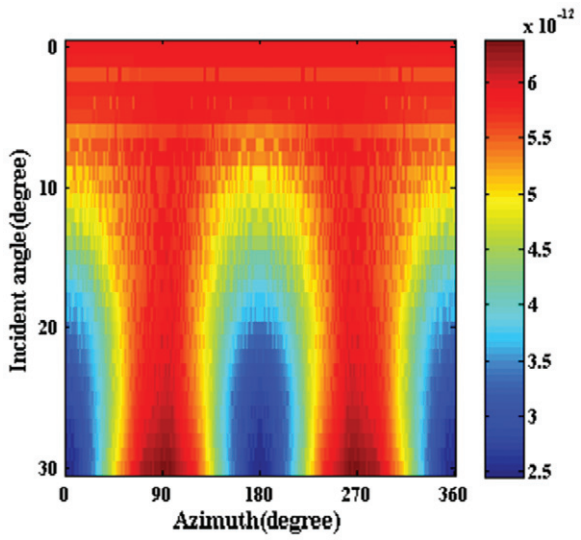

Figure 7. Difference of reflection responses versus incident angle and azimuth for the parallel fracture model and HTI medium model (small-scale fractures gas-filled). The response was derived from the *Z*-component of the data.

fractures. Figures 7 and 8 show that the influence derived for the perpendicular large-scale fracture model is larger than for the parallel large-scale fracture. In order to invert for small-scale fracture information for the parallel or perpendicular fracture model, it will be better if we can reduce the effect on reflection information derived from large-scale fractures. Using the difference of reflection response at two azimuths can reduce most of the influence caused by large-scale fractures at near zero offset. Although this method could not work well when the incident angle increases, it still reduces some influence caused by large-scale fractures.

To study the effects of large-scale fractures on our ability to characterize the small-scale fractures, we vary the large-scale fracture compliances from $0.02 \times 10^{-9}\,\mathrm{m\,Pa^{-1}}$ to

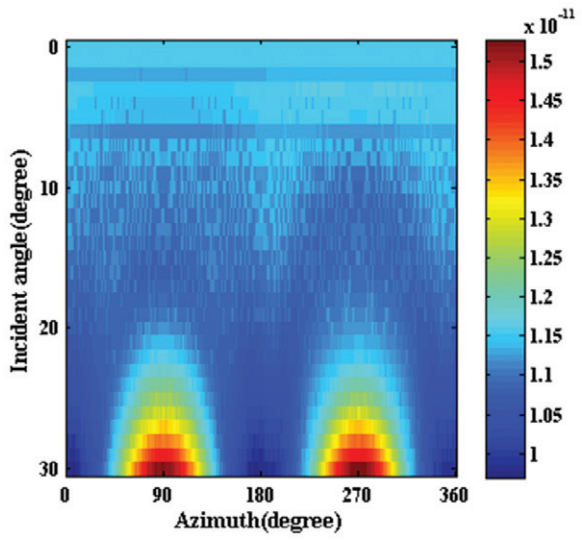

Figure 8. Same as figure 7 but for the perpendicular fracture model.

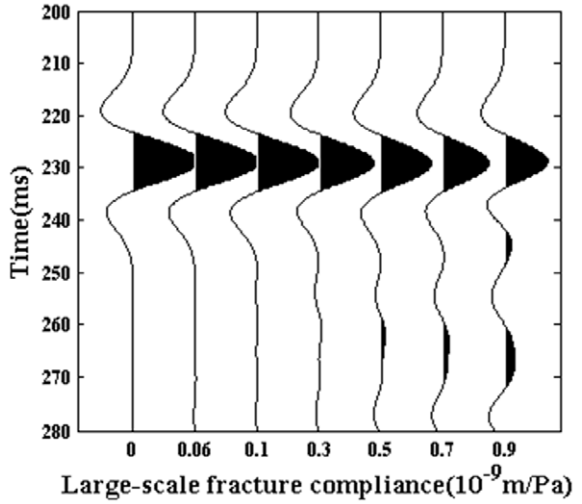

Figure 9. *Z*-component of motion for the P-wave reflected for the parallel fracture model. The small-scale fracture is gas-filled. Results for compliance varying from 0 (e.g. no large-scale fractures) to $0.9 \times 10^{-9}\,\mathrm{m\,Pa^{-1}}$ are shown. Offset is 400 m. Azimuth is 30°.

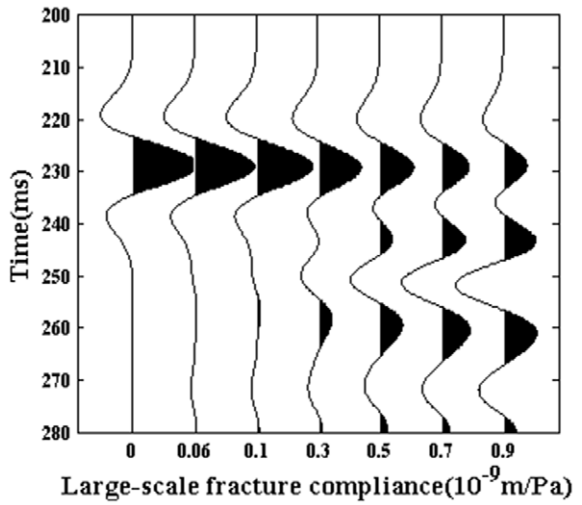

Figure 10. Same as figure 9 but for the perpendicular fracture model.

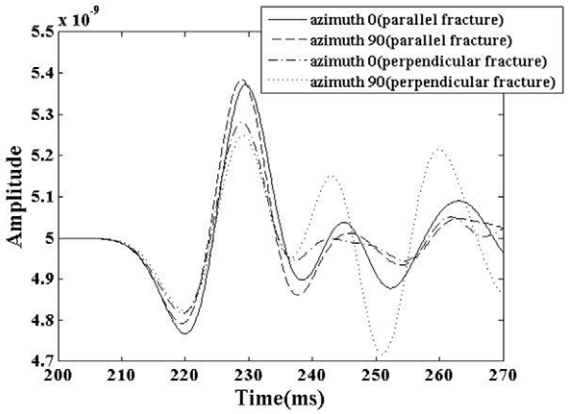

Figure 11. P-wave reflection waveforms (Z-component). Z_N and Z_T is $0.6 \times 10^{-9}\,\mathrm{m\,Pa^{-1}}$. Offset is 400 m.

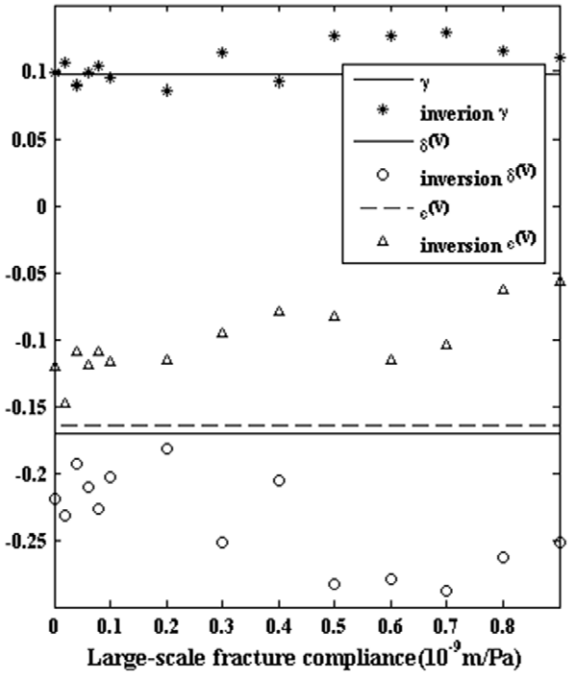

Figure 12. Inversion Thomsen-type anisotropy parameters for the parallel fracture model. The small-scale fracture is gas-filled.

$0.9 \times 10^{-9}\,\mathrm{m\,Pa^{-1}}$. Figures 9 and 10 show synthetic seismic data for the model where the large-scale fractures strike parallel to the strike of the small-scale fractures and where the large-scale fractures are perpendicular to the small-scale fractures, respectively. Reflection amplitude goes down and scattered wave energy goes up as fracture compliance increases. Scattered wave energy is not remarkable until fracture compliance is larger than $0.1 \times 10^{-9}\,\mathrm{m\,Pa^{-1}}$ for both the parallel fracture model and the perpendicular fracture model. This suggests that large-scale fractures would seriously affect reflection information when large-scale fracture compliance is larger than $0.1 \times 10^{-9}\,\mathrm{m\,Pa^{-1}}$. What is more, the scattered waves caused by perpendicular fractures are much more complicated than those caused by parallel fractures.

Figure 11 compares vertical-component waveforms at two receivers when large-scale fracture compliance is

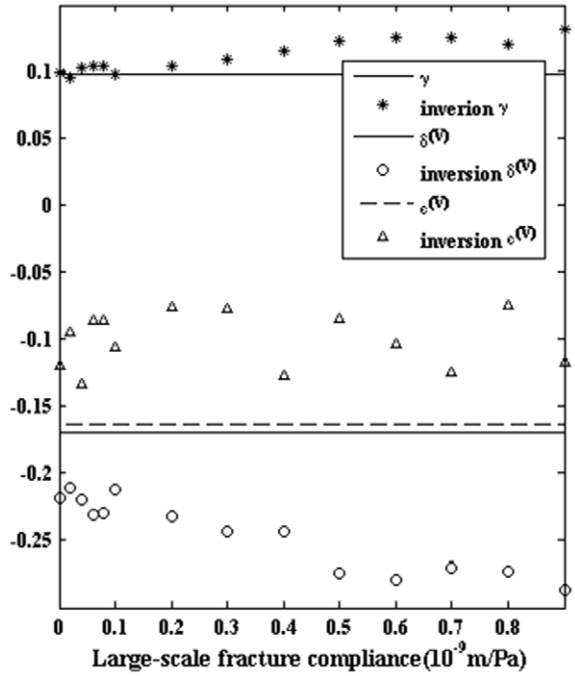

Figure 13. Inversion Thomsen-type anisotropy parameters for the perpendicular fracture model. Small-scale fractures are gas-filled.

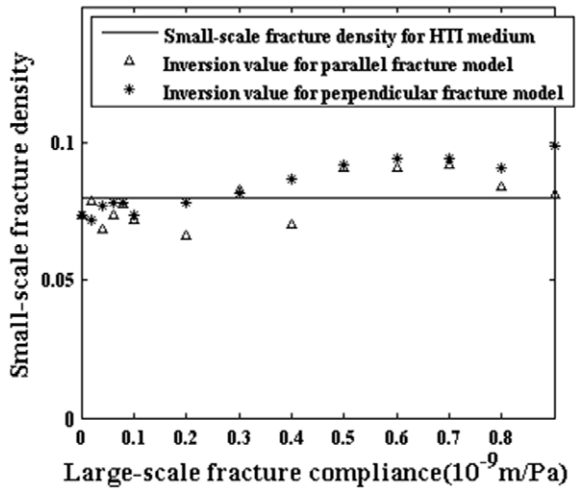

Figure 14. Inversion result for small-scale fracture density. Small-scale fractures are gas-filled.

$0.6 \times 10^{-9}\,\mathrm{m\,Pa^{-1}}$. Small-scale fractures dominate the behavior of the first reflection pulse. Absolute amplitude for azimuth 0 degrees is larger than for azimuth 90 degrees in the first reflection pulse. This result is coincident with what we discussed before when there are only small-scale fractures. However, properties of the scattered waves are mainly governed by large-scale fracture. For the parallel fracture model, amplitude of the scattered wave for azimuth 0 degrees is still larger than the one for azimuth 90 degrees. For the perpendicular fracture model, amplitude of the scattered wave for azimuth 0 degrees is less than the one for azimuth 90 degrees. According to our previous discussion, it should be possible to use reflection amplitude azimuth characteristics to evaluate

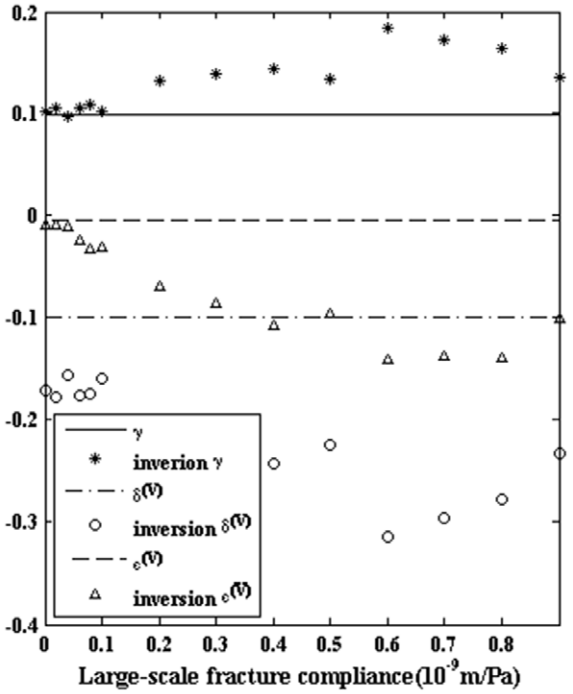

Figure 15. Inversion Thomsen-type anisotropy parameters for the fracture model. Small-scale fractures are water-filled.

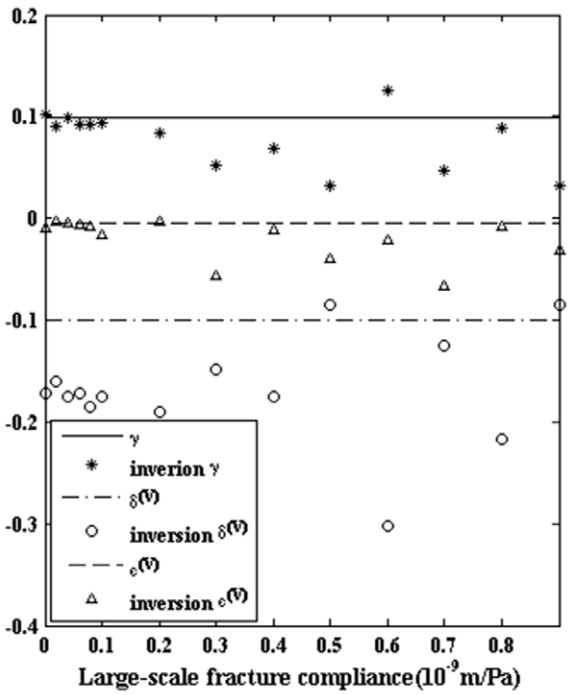

Figure 16. Inversion Thomsen-type anisotropy parameters for the perpendicular fracture model. Small-scale fractures are water-filled.

small-scale fracture orientation and the strike of the large-scale fractures can be estimated from the scattered waves.

4. Inversion results analysis

We can, based on equation (4), use a genetic algorithm to invert for Thomsen-type anisotropy parameters (γ,$\delta^{(V)}$ and

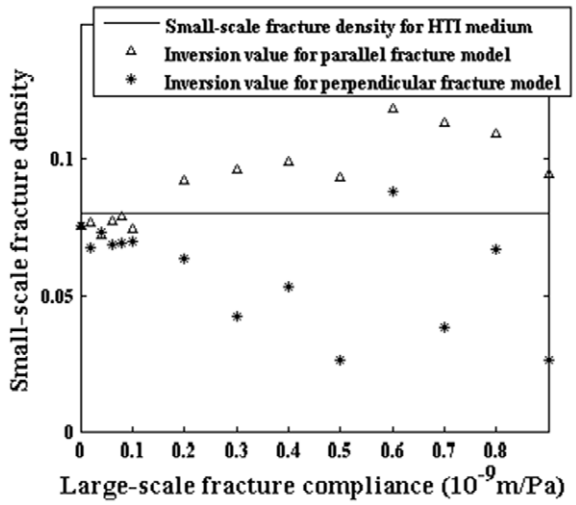

Figure 17. Inversion result for small-scale fracture density. Small-scale fractures are water-filled.

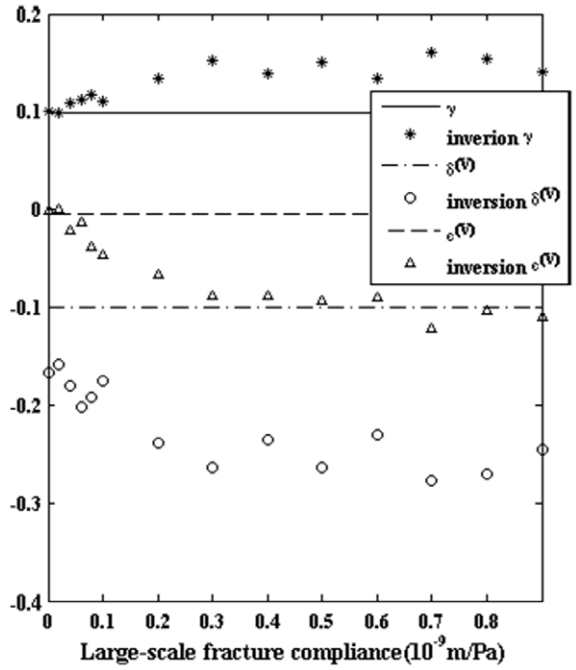

Figure 18. Inversion Thomsen-type anisotropy parameters for the parallel fracture model. Small-scale fractures are filled with carbon dioxide.

$\varepsilon^{(V)}$). In figures 12 and 13, we show the inversion results for parallel fracture and perpendicular fracture models when the small-scale fracture is gas-filled, respectively. It is interesting to note that the inversion results for γ are much better than those for the other anisotropy parameters ($\delta^{(V)}$ and $\varepsilon^{(V)}$). For the parallel fracture model, the error of the inversion for γ is less than 10% when large-scale fracture compliance is more than $0.1 \times 10^{-9}\,\mathrm{m\,Pa^{-1}}$. Precision of inversion for γ decreases when large-scale fracture compliance is more than $0.1 \times 10^{-9}\,\mathrm{m\,Pa^{-1}}$. The maximum error of inversion for γ is 30% when large-scale fracture compliance is $0.7 \times 10^{-9}\,\mathrm{m\,Pa^{-1}}$. For the perpendicular fracture model,

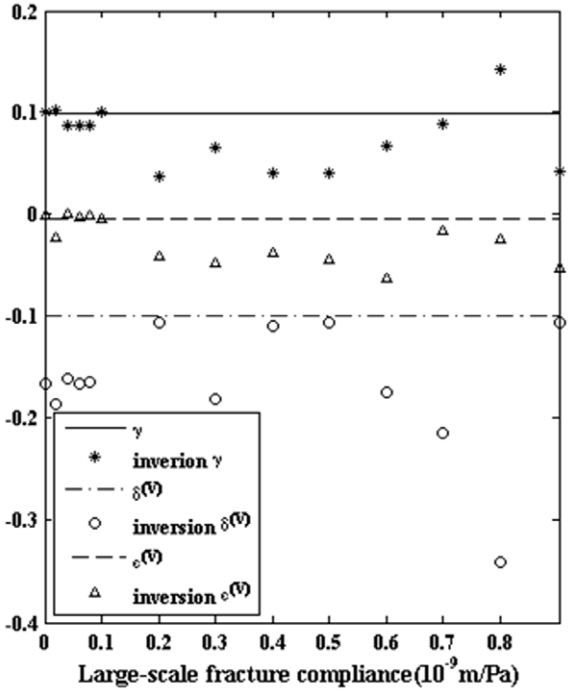

Figure 19. Inversion Thomsen-type anisotropy parameters for the perpendicular fracture model. Small-scale fractures are filled with carbon dioxide.

the error of inversion for γ is less than 10% when large-scale fracture compliance is less than $0.2 \times 10^{-9}\,\mathrm{m\,Pa^{-1}}$. The error increases with the growth of fracture compliances which are larger than $0.2 \times 10^{-9}\,\mathrm{m\,Pa^{-1}}$. The maximum error of inversion for γ is 35% when fracture compliance is $0.9 \times 10^{-9}\,\mathrm{m\,Pa^{-1}}$.

According to the relationship between generic Thomsen parameter γ and crack density (equations (2) and (6)), we can estimate small-scale fracture density based on inversion for γ. Figure 14 shows the sensitivity of fracture compliance to estimated crack density when small-scale fractures are gas-filled. For the parallel fracture model, the error of estimated small-scale fracture density is less than 10% when large-scale fracture compliance is below $0.1 \times 10^{-9}\,\mathrm{m\,Pa^{-1}}$, and we expect that it is 14% while large-scale fracture compliance is $0.04 \times 10^{-9}\,\mathrm{m\,Pa^{-1}}$. The maximum error of estimated small-scale fracture density is 17% when fracture compliance is $0.2 \times 10^{-9}\,\mathrm{m\,Pa^{-1}}$. For the perpendicular fracture model, the error of estimated small-scale fracture density is less than 10% when large-scale fracture compliance is less than $0.4 \times 10^{-9}\,\mathrm{m\,Pa^{-1}}$ and the maximum error is 24% while the large-scale fracture compliance is $0.9 \times 10^{-9}\,\mathrm{m\,Pa^{-1}}$. For both the parallel fracture model and the perpendicular fracture model, it is almost possible to evaluate small-scale fracture density when large-scale fracture compliance is less than $0.1 \times 10^{-9}\,\mathrm{m\,Pa^{-1}}$ while small-scale fractures are filled with gas. As figures 17 and 20 show, if large-scale fracture compliance is less than $0.1 \times 10^{-9}\,\mathrm{m\,Pa^{-1}}$, estimating small-scale fracture density will still work well when small-scale fracture is filled with water and carbon dioxide, respectively. We have thus found that, regardless of the orientation of large-scale fractures we can determine the fracture density of the

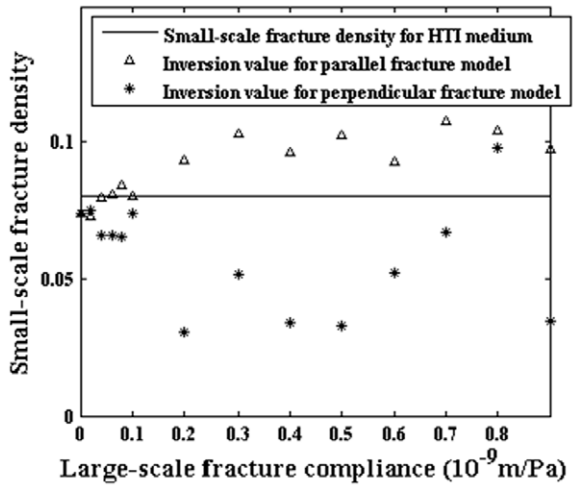

Figure 20. Small-scale fractures density inversion result. The small-scale fracture is filled with carbon dioxide.

small-scale fractures when the large-scale fracture compliance is less than $0.1 \times 10^{-9}\,\mathrm{m\,Pa^{-1}}$.

In figures 15, 16, 18 and 19, we show the inversion results for parallel fracture or perpendicular fracture models when small-scale fractures are filled with water and carbon dioxide, respectively. The inversion results for $\varepsilon^{(V)}$ are better and more stable when large-scale fracture compliance is less than $0.1 \times 10^{-9}\,\mathrm{m\,Pa^{-1}}$ than the ones when large-scale fracture compliance is larger than $0.1 \times 10^{-9}\,\mathrm{m\,Pa^{-1}}$. The inversion results for $\varepsilon^{(V)}$ always have large errors no matter what fluid fills the small-scale fractures, but the inversion results for $\varepsilon^{(V)}$ have a big change when the small-scale fractures are filled with gas in comparison with the ones when the small-scale fractures are fluid-filled. Take two parallel fracture models as examples (figures 12 and 18), the ranges of inversion results for $\varepsilon^{(V)}$ are -0.1095 and -0.1474 when large-scale fracture compliance is less than $0.1 \times 10^{-9}\,\mathrm{m\,Pa^{-1}}$ while the ones for small-scale fracture filled with carbon dioxide are -0.001 and -0.0469, so the differences of inversion results for $\varepsilon^{(V)}$ are about 0.1 which can be considered a big change.

5. Conclusions

We have used numerical simulation and inversion to investigate the ability to infer anisotropy parameters for media containing aligned small-scale and large-scale fractures. The small-scale fractures lead to an equivalent HTI medium and the large-scale fractures cause scattering of the seismic waves. We investigated cases where the large-scale fractures are either parallel or perpendicular to the small-scale fractures. Visual inspection of the simulated traces shows that the scattering from the large-scale fractures does not noticeably influence the character of the waveforms when compliance is less than about $0.1 \times 10^{-9}\,\mathrm{m\,Pa^{-1}}$. While our results depend on several model parameters and the acquisition scenario, they do lead us to believe that AVAZ can often be reliable for estimating the fracture density of small-scale fractures even when large-scale fractures are present. Inversion results for

Thomsen-type anisotropy parameter $\varepsilon^{(V)}$ have large differences when the small-scale fracture change from gas-filled to fluid-filled if large-scale fracture compliance is less than $0.1 \times 10^{-9}\,\mathrm{m\,Pa^{-1}}$.

Acknowledgments

The work was supported by the National Basic Research Program of China (No. 2014CB239104 and No. 2012CB214800) and National Science and Technology Major Project of the Ministry of Science and Technology of China (No. 2011ZX05066-002). Additional support came from the Founding Member Program of the Earth Resources Laboratory at MIT.

References

Bakulin A, Grechka V and Tsvankin I 2000 Estimation of crack parameters from reflection seismic data–part I: HTI model due to a single crack set *Geophysics* **65** 1788–802

Coates R and Schoenberg M 1995 Finite difference modeling of faults and fractures *Geophysics* **60** 1514–26

Fang X, Fehler M, Burns D and Zhu Z 2013a Sensitivity analysis of fracture scattering, *Geophysics* **78** T1–10

Fang X, Fehler M, Zhu Z and Zheng Y 2013b Reservoir fracture characterizations from seismic scattered waves *SEG Expanded Abstracts* **82** 1–6

Gutierrez I V 2009 Fracture studies from amplitude versus offset and azimuth and vertical seismic profile data *Thesis* University of Edinburgh

Hall S and Kendall J M 2003 Fracture characterization at Valhall: application of P-wave amplitude variation with offset and azimuth (AVOA) analysis to a 3D ocean-bottom data set *Geophysics* **68** 1150–60

Hudson J A 1980 Overall properties of a cracked solid Math *Proc. Camb. Phil. Soc.* **88** 371–84

Hudson J A 1981 Wave speeds and attenuation of elastic waves in material containing cracks *Geophys. J. R. Astron. Soc.* **64** 133–50

Hudson J A, Liu E and Crampin S 1996 The mechanical properties of materials with interconnected cracks and proes *Geophys. J. Int.* **124** 105–12

Jakobsen M, Liu E and Chapman M 2007 Estimation of anisotropic permeability in fractured reservoirs from seismic AVOZ analysis *SEG Expanded Abstracts* 99–103

Liu Y, Fehler M, Fang X and Liu C 2013a Estimating the fracture density of small-scale vertical fractures when large-scale vertical fractures are present *SEG Expanded Abstract* 393–7

Liu E, Hudson J and Pointer T 2000 Equivalent medium representation of fractured rock *J. Geophys. Res.* **105** 2981–3000

Liu C, Liu Y, Feng X and Lu Y 2012 Constructing the convex quadratic function for the evaluation of crack density of HTI media using P- and converted waves *J. Geophys. Eng.* **9** 729–35

Luo M and Evans B J 2004 An amplitude-based multiazimuth approach to mapping fractures using P-wave 3D seismic data *Geophysics* **69** 690–8

Rüger A 1996 Reflection coefficients and azimuthal AVO analysis in anisotropic media *Doctoral Dissertation* Colorado School of Mines

Rüger A 1997 P-wave reflection coefficients for transversely isotropic models with vertical and horizontal axis of symmetry *Geophysics* **62** 713–22

Rüger A and Tsvankin I 1995 Azimuthal variation of AVO response for cracked reservoirs *SEG Expanded Abstracts* **65** 1103–6

Schoenberg M 1980 Elastic wave behavior across linear slip interfaces *J. Acoust. Soc. Am.* **68** 1516–21

Schoenberg M 1983 Reflection of elastic waves from periodically stratified media with interfacial slip *Geophys. Prospect.* **31** 265–92

Thomsen L 1986 Weak elastic anisotropy *Geophysics* **51** 1954–66

Thomsen L 1988 Reflection seismology over azimuthally anisotropic media *Geophysics* **53** 304–13

Thomsen L 1995 Elastic anisotropy due to aligned cracks in porous rock *Geophys. Prospect.* **43** 805–29